

Resonant Inelastic X-Ray Scattering Reveals Hidden Local Transitions of the Aqueous OH Radical

L. Kjellsson,¹ K. D. Nanda,² J.-E. Rubensson,¹ G. Doumy,³ S. H. Southworth,³ P. J. Ho,³ A. M. March,³ A. Al Haddad,³ Y. Kumagai,³ M.-F. Tu,³ R. D. Schaller,^{4,5} T. Debnath,⁶ M. S. Bin Mohd Yusof,⁶ C. Arnold,^{7,8,9} W. F. Schlotter,¹⁰ S. Moeller,¹⁰ G. Coslovich,¹⁰ J. D. Koralek,¹⁰ M. P. Minitti,¹⁰ M. L. Vidal,¹¹ M. Simon,¹² R. Santra,^{7,8,9} Z.-H. Loh,⁶ S. Coriani,¹¹ A. I. Krylov,^{2,*} and L. Young^{3,13,†}

¹*Department of Physics and Astronomy, Uppsala University, Box 516, S-751 20 Uppsala, Sweden*

²*Department of Chemistry, University of Southern California, Los Angeles, California 90007, USA*

³*Chemical Sciences and Engineering Division, Argonne National Laboratory, Lemont, Illinois 60439, USA*

⁴*Center for Nanoscale Materials, Argonne National Laboratory, Lemont, Illinois 60439, USA*

⁵*Department of Chemistry, Northwestern University, Evanston, Illinois 60208, USA*

⁶*Division of Chemistry and Biological Chemistry, Nanyang Technological University, Singapore 639798*

⁷*Center for Free-Electron Laser Science, DESY, 22607 Hamburg, Germany*

⁸*Department of Physics, Universität Hamburg, 20146 Hamburg, Germany*

⁹*Hamburg Centre for Ultrafast Imaging, 22607 Hamburg, Germany*

¹⁰*LCLS, SLAC National Accelerator Laboratory, Menlo Park, California 94025, USA*

¹¹*DTU Chemistry—Department of Chemistry, Technical University of Denmark, DK-2800 Kongens Lyngby, Denmark*

¹²*Sorbonne Université and CNRS, Laboratoire de Chimie Physique-Matière et Rayonnement, 75252 Paris Cedex 05, France*

¹³*Department of Physics and James Franck Institute, The University of Chicago, Chicago, Illinois 60637, USA*



(Received 8 March 2020; revised manuscript received 1 May 2020; accepted 22 May 2020; published 12 June 2020)

Resonant inelastic x-ray scattering (RIXS) provides remarkable opportunities to interrogate ultrafast dynamics in liquids. Here we use RIXS to study the fundamentally and practically important hydroxyl radical in liquid water, OH(*aq*). Impulsive ionization of pure liquid water produced a short-lived population of OH(*aq*), which was probed using femtosecond x-rays from an x-ray free-electron laser. We find that RIXS reveals localized electronic transitions that are masked in the ultraviolet absorption spectrum by strong charge-transfer transitions—thus providing a means to investigate the evolving electronic structure and reactivity of the hydroxyl radical in aqueous and heterogeneous environments. First-principles calculations provide interpretation of the main spectral features.

DOI: 10.1103/PhysRevLett.124.236001

The hydroxyl radical (OH) is of major importance for atmospheric, astrochemical, biological, industrial, and environmental research. In the gas phase, OH is the primary oxidizing agent that rids the atmosphere of volatile organic compounds and other pollutants [1]. It is a key tracer describing the evolution and thermodynamics of interstellar clouds [2]. Despite its reactive nature stemming from an open electronic shell, the gas-phase absorption spectrum of OH has been fully characterized in the microwave [3], infrared, optical or ultraviolet (UV) [4], and, more recently, the x-ray [5] spectral ranges. Beyond purely gas-phase processes, these OH fingerprints also characterize heterogeneous processes such as the generation of reactive oxygen species from photocatalysis [6].

Spectroscopic characterization of the hydroxyl radical in the condensed phase is more challenging, owing to its extreme reactivity and short lifetime. Of particular interest is the characterization of OH in aqueous environments, which impacts radiation biology [7] and chemistry [8]. Given its unpaired spin, electron spin resonance techniques

are a natural choice to detect the presence of OH, either directly or through spin traps, but only microsecond timescales are accessible [6]. For faster timescales, desired for tracking reaction dynamics, one may consider UV spectroscopy. The UV spectrum of solvated OH obtained via pulsed radiolysis of water [9] is reproduced in Fig. 1. It is dominated by a strong feature at 230 nm (5.4 eV), whereas the dominant gas-phase absorption at 309 nm (4 eV), due to valence excitation from the ground (*X*) to the lowest excited electronic state (*A*), is barely visible. On the basis of electronic structure calculations [10–13], this dominant spectral feature of OH(*aq*) was attributed to charge-transfer (CT) transitions from the lone pair of nearby waters, filling the hole in the OH 1π orbital (Fig. 1, bottom left).

Resonant inelastic x-ray scattering (RIXS) delivers atomic-site specific information about the local electronic structure and dynamics in condensed phase. The application of soft x-ray RIXS to liquids [14] has generated considerable attention; improvements in sensitivity [15] and energy resolution [16] continue to open new perspectives on

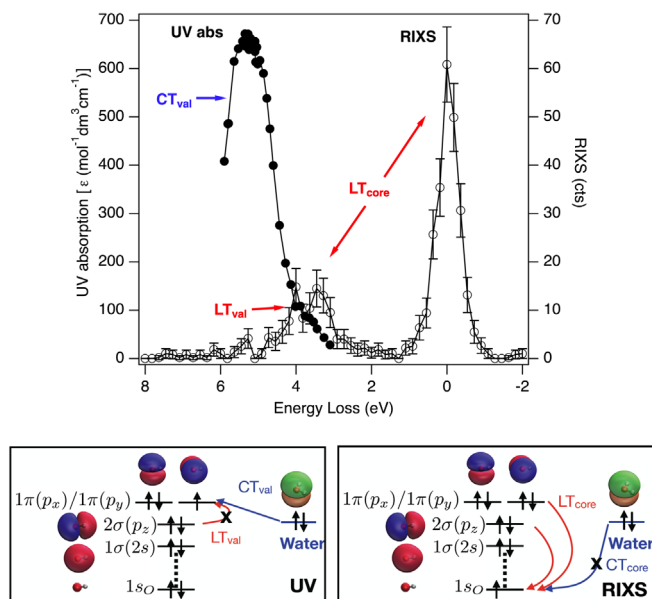


FIG. 1. UV absorption and RIXS energy-loss spectra of $\text{OH}(aq)$ (top) and molecular orbital diagrams (bottom). The electronic configuration of OH is $1s_O^2 1\sigma^2 2\sigma^2 1\pi^3$. The lowest valence transition ($2\sigma \rightarrow 1\pi$, marked as LT_{val} for local transition) has low oscillator strength due to its $p_z \rightarrow p_x/p_y$ character; the UV spectrum is dominated by charge-transfer transition (CT_{val}) from nearby waters. In resonantly excited OH ($1s_O^1 1\sigma^2 2\sigma^2 1\pi^4$), both $1\pi \rightarrow 1s$ and $2\sigma \rightarrow 1s$ transitions are bright, giving rise to the elastic peak (zero energy loss) and a feature at ~ 4 eV. The gap between the two RIXS peaks corresponds to the $2\sigma \rightarrow 1\pi$ energy.

fundamental liquid-phase interactions [17–19]. Recently, the combination of RIXS, liquid microjets, and x-ray free-electron lasers enabled time-resolved measurements of electronic structure of transient species in solutions [20,21].

Here we report the RIXS spectrum for the short-lived OH radical in water (Fig. 1). In sharp contrast to the UV spectrum, the RIXS spectrum of $\text{OH}(aq)$ features two peaks corresponding to transitions between the OH orbitals (Fig. 1, bottom right). The energy difference between the elastic and inelastic peaks corresponds to the $X \rightarrow A$ transition, which, in turn, roughly equals the energy gap between the 2σ and 1π orbitals. Thus, RIXS reveals intrinsic local electronic structure of solvated OH , which is obscured in the UV region by CT transitions. In contrast to CT transitions, which are characteristic of the solvent and its local structure, local transitions (LT) are fingerprints of the solute and can, therefore, be used to track reactive hydroxyl radicals in various complex and heterogeneous environments. The CT transitions in the RIXS spectrum are suppressed because the compact shape of the core $1s_O$ orbital results in poor overlap with the lone pairs of neighboring waters. We confirm this by *ab initio* RIXS calculations using a new electronic structure method [22,23] based on the equation-of-motion coupled-cluster

(EOM-CC) theory. These calculations also reproduce the relative RIXS line intensities, positions, and widths for the elastic and inelastic peaks of $\text{OH}(aq)$ and $\text{OH}^-(aq)$.

The $\text{OH}(aq)$ spectra are also compared to the x-ray emission spectra (XES) of liquid water, where the role of hydrogen bonding and ultrafast dynamics has long been debated [15,18,24–28]. If core-ionized water dissociates prior to core-hole decay, a core-excited $\text{OH}(aq)$ is formed in the $1s_O^1 1\sigma^2 2\sigma^2 1\pi^4$ intermediate RIXS state (Fig. 1). The lower-energy component of the water XES doublet has been attributed to this ultrafast dissociation [15] and our measurement of the position of the $\text{OH}(aq)$ RIXS resonance directly provides relevant information that previously was indirectly deduced [27].

Here, as in our companion study using x-ray transient absorption (XTAS) [29], strong-field ionization is used to create the hydroxyl radical in pure liquid water. After initial formation of a water cation (H_2O^+) ultrafast proton transfer to a neighboring water molecule on a sub-100 fs timescale [30] creates the hydroxyl radical, $\text{OH}(aq)$, and the hydronium ion (H_3O^+). In the time window between proton transfer (~ 100 fs) and geminate recombination (~ 20 ps), the ionized liquid water sample contains $\text{OH}(aq)$. Previously [29], we used XTAS to probe the kinetics of $\text{OH}(aq)$, a study facilitated by the fact that the resonant $1s_O \rightarrow 1\pi$ transition of $\text{OH}(aq)$ occurs cleanly in the “water window,” i.e., below the liquid water absorption edge. Here we report on our simultaneous use of RIXS to probe $\text{OH}(aq)$, thus allowing spectroscopic investigation of local valence transitions that are chemically most relevant.

Briefly, optical-pump x-ray-probe RIXS was performed using the soft x-ray research (SXR) instrument [30] at the Linac coherent light source (LCLS) at SLAC National Accelerator Laboratory. Monochromatized x-ray pulses were scanned from 518 to 542 eV (~ 10 μJ , ~ 40 fs, 200 meV bandwidth). Three photon detection channels were simultaneously recorded: transmission, total fluorescence, and dispersed emission. A detailed description of the performance of the optical laser, water jet, and x-ray monochromator calibration, shot-by-shot normalization procedures can be found in [29]. Here we describe additionally the x-ray emission spectrometer and experimental geometries for RIXS measurements of $\text{OH}(aq)$.

X-ray emission was collected perpendicular to the incoming x-ray beam and along the x-ray polarization axis to suppress elastic scattering using a variable-line-spacing grating-based spectrometer with an efficiency of $\sim 10^{-7}$ [31]. The low collection efficiency for the RIXS spectrum combined with a limited collection time precluded binning of these RIXS spectra with the 40-fs, 200-meV time and energy resolutions associated with the XFEL pulse. A CCD camera located at the exit plane of the spectrometer recorded images on a shot-by-shot basis. The energy dispersion and absolute energy of the incoming monochromatized radiation

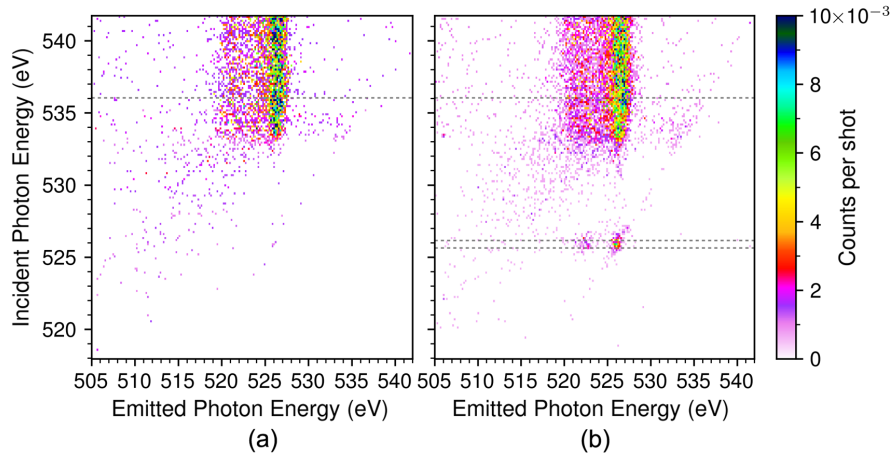


FIG. 2. RIXS maps of ionized liquid water (a) before valence ionization and (b) after valence ionization, integrated for time delays between 200–1400 fs. The intensity of the maps is the number of counts on the emission spectrometer (15 054) normalized by the number of XFEL pulses (365 846). Before ionization, a threshold for emission is seen near 534 eV incident photon energy. After ionization, a resonant feature appears at 526 eV due to the transient $\text{OH}(aq)$ radical. The two energy windows used to create the spectra shown in Fig. 3 are marked: 536–542 eV for bulk water and 525.70–526.12 eV for $\text{OH}(aq)$.

were previously calibrated [29,32]. The dispersion of the emission spectrometer was determined by fitting a first degree polynomial to the elastic line visible in Fig. 2(b).

To gain insight into the nature of main spectral features, we carried out electronic structure calculations using EOM-CC [33] with single and double excitations (EOM-CCSD) augmented by core-valence separation (CVS) [34] to enable access to core-level states [22,35]. As a multistate method, EOM-CC treats different valence and core-level states on an equal footing and is particularly well suited for modeling molecular properties, including nonlinear properties [33,36–38]. To account for solvent effects, the spectral calculations of $\text{OH}(aq)/\text{OH}^-(aq)$ were carried out within the QM/MM (quantum mechanics-molecular mechanics) scheme with water molecules described by classical force field and OH/OH^- described by EOM-CCSD by using snapshots from equilibrium *ab initio* molecular dynamics simulations.

The electronic factors entering RIXS cross sections are the RIXS transition moments given by the following Kramers-Heisenberg-Dirac (KHD) expression [39]:

$$M_{fg}^{xy} = -\sum_n \left(\frac{\langle f | \mu^y | n \rangle \langle n | \mu^x | g \rangle}{\Omega_{ng} - \omega_{i,x} - i\epsilon_n} + \frac{\langle f | \mu^x | n \rangle \langle n | \mu^y | g \rangle}{\Omega_{ng} + \omega_{o,y} + i\epsilon_n} \right),$$

where g and f denote the initial and final electronic states (i.e., ground and valence excited state of OH), ω_i/ω_o are the incoming/outgoing photon frequencies, and the sum runs over all electronic states; $\Omega_{ng} = E_n - E_g$ is the energy difference between states n and g , and $i\epsilon_n$ is the imaginary inverse lifetime parameter for state n . In the present experiment, the dominant contribution to the RIXS cross section comes from the term corresponding to the $1s^1_O, \dots, 1\pi^4$ state, which is resonant with excitation

frequency of 526 eV, such that the spectra can be qualitatively understood within a three-state model. Within the EOM-CC framework, the KHD expression is evaluated using EOM-CC energies and wave functions. Rather than arbitrarily truncating the sum over states, we replace all ϵ_n s with a phenomenological damping factor ϵ and use damped response theory to convert the KHD expression into a numerically tractable closed form [23,37,40]. Robust convergence of the auxiliary response equations is achieved by using CVS within the damped response domain [23]. The resulting method combines rigorous treatment of RIXS cross sections and high-level description of electron correlation. To describe vibrational structure in the RIXS spectrum, we computed Franck-Condon factors (FCFs) using three-state model (as was done in Ref. [17]) and harmonic approximation. To quantify the relative strengths of LT and CT transitions, we also carried out calculations on model water-OH structures. All calculations were performed using the Q-Chem electronic structure package [41]. Full details of computational protocols are given in the Supplemental Material [42].

Theoretical estimates of key structural parameters of the isolated OH given in Table I agree well with experimental values [4,5]. Theory overestimates the energy of the valence transition by 0.08 eV and underestimates the energy of the core-excited state by 0.7 eV; these differences are within the error bars of the method [22]. The variations in bond lengths and frequencies among different states are consistent with the molecular orbital picture of the electronic states. The structural differences between the states give rise to a vibrational progression in the x-ray absorption spectrum; the computed FCFs are in excellent agreement with the experimental ones (see the Supplemental Material [42]).

TABLE I. Key structural parameters of isolated OH radical.

State	Character	T_e , eV	r_e , Å	ω_e , eV	μ , a.u.	
$X(^2\Pi_1)$	$1s^2 1\sigma^2 2\sigma^2 1\pi^3$	0.000	0.972	0.468	0.701	^a
		0.000	0.970	0.463		^b
core $^2\Sigma^+$	$1s^{-1} 1\sigma^2 2\sigma^2 \pi^4$	525.1	0.916	0.543	0.814	^a
		525.8	0.915	0.533		^c
$A(^2\Sigma^+)$	$1s^2 1\sigma^2 2\sigma^1 1\pi^4$	4.128	1.014	0.398	0.801	^a
		4.052	1.012	0.394		^b

^aTheory, this Letter. Energies (T_e) and dipole moments (μ): (cvs)-EOM-EE-CCSD, computed at the experimental geometries; r_e and ω_e : (cvs)-EOM-IP-CCSD. Basis set: uC-6-311(2+, +)G(2df, p).

^bExperiment Ref. [4].

^cExperiment Ref. [5].

Figure 2 shows the RIXS maps before and after the ionization pulse. The RIXS map prior to ionization, Fig. 2(a), is in agreement with earlier measurements [15,24,26]. There is a threshold for emission at ~ 534 eV excitation energy and a pre-edge peak at 535 eV. After

ionization, Fig. 2(b), a new resonant feature appears at 526 eV excitation energy that is identified as $1s_O \rightarrow 1\pi$ transition of $\text{OH}(aq)$: its position is near that of gas-phase OH [5] and its kinetics are consistent with proton transfer [29]. The position of the quasielastic RIXS line of $\text{OH}(aq)$ coincides with the lower-energy component of the water XES doublet (see dashed line in Fig. 3), providing a check on the absolute energy and consistent with the interpretation [15] of this peak as due to ultrafast dissociation.

Table II summarizes the main RIXS features of $\text{OH}(aq)$ and $\text{OH}^-(aq)$, comparing experimental and theoretical values. The RIXS spectrum has a peak with 0.7 eV FWHM that is assigned to quasielastic $GS \rightarrow 1s_O^{-1}\pi^{+1} \rightarrow GS$ scattering to the electronic ground state. We also observe a 1.5 eV wide structure beginning at 3.6 eV energy loss that corresponds to scattering to the first electronically excited state: $GS \rightarrow 1s_O^{-1}\pi^{+1} \rightarrow 2\sigma^{-1}\pi^{+1}$. The calculations reproduce the gap (ΔE) between the quasielastic and energy-loss peak well; however, the absolute position of the $1s_O \rightarrow 1\pi$ transition is 1 eV off. EOM-EE-CCSD excitation spectra for core-level transitions often exhibit systematic shifts of 0.5–1.5 eV, attributed to insufficient treatment of electron correlation [22], whereas the relative positions of the peaks are reproduced with higher accuracy. The intensity ratio of the two peaks stems from their π and σ character and is reproduced qualitatively by our calculations.

Both quasielastic and energy-loss peaks are broadened due to the interaction with polar solvent and to vibrational structure. As shown in Table I, the dipole moment in electronically excited OH is 14% larger than in the ground state, suggesting larger inhomogeneous broadening for the energy-loss peak; this is confirmed by our QM/MM calculations, where the effect of the solvent is treated explicitly. The analysis of structural differences between the ground $X(^2\Pi_1)$, valence excited $A(^2\Sigma^+)$, and core-excited states suggests longer vibrational progression for the energy-loss peak, which is confirmed by the computed FCFs (see the Supplemental Material [42]). This trend can be rationalized by the shapes of molecular orbitals: the

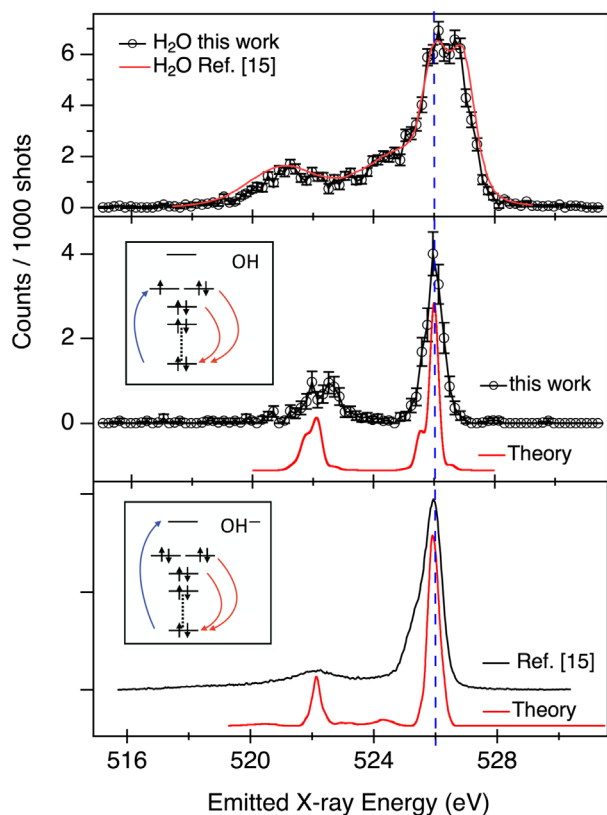


FIG. 3. Comparison of RIXS from OH and OH^- . Top: Experimental XES from water for excitation energies between 536–542 eV compared to XES of water excited at 550.1 eV [15]. Middle: RIXS from the 526-eV resonance of $\text{OH}(aq)$ compared with theory (shifted +1.0 eV). Bottom: RIXS from OH^- excited at 533.5 eV and compared with theory (shifted -0.2 eV). Ref. [15] data shifted -0.7 eV. Insets show molecular orbital diagrams for the RIXS transitions in OH and OH^- .

TABLE II. Positions and relative intensities of the RIXS peaks for OH(*aq*) and OH⁻(*aq*) as defined in the insets of Fig. 3.

Species	Source	E , eV	ΔE , eV	Ratio
OH(<i>aq</i>)	This work ^a	526.0	-3.8	2.1
OH(<i>aq</i>)	This work ^b	525.0	-4.0	2.04
OH ⁻ (<i>aq</i>)	Ref. [15].	526.5	-3.8	4.3
OH ⁻ (<i>aq</i>)	This work ^b	526.2	-3.8	5.20

^aExperiment.^bTheory.

bonding character of 2σ orbital involved in the $GS \rightarrow 1s_O^{-1}\pi^{+1} \rightarrow 2\sigma^{-1}\pi^{+1}$ transition renders it more sensitive to vibrational excitations.

The middle and bottom panels of Fig. 3 compare the RIXS of OH(*aq*) to that of OH⁻(*aq*) [15]. The two species show very similar emission spectra, as expected from the similarity of the intermediate RIXS state. There is a significant difference in the intensities of the quasielastic π peak and the energy-loss (σ) feature. The observed π/σ ratios for OH(*aq*) and OH⁻(*aq*) are 2.1:1 and 4.3:1, compared to the calculated 2.04:1 and 5.20:1. In OH⁻ calculations, we assumed resonant excitation to the lowest XAS peak of solvated OH⁻, which roughly corresponds to the transition to a diffuse σ -type orbital. The observed π/σ RIXS ratio from OH⁻(*aq*) depends strongly on the nature of the intermediate state and, therefore, would be very sensitive to the excitation frequency; thus, the discrepancy between the computed values and Ref. [15] could be due to different excitation regimes.

To rationalize the apparent absence of the CT_{core} transitions in RIXS, we computed valence and core-level transitions for model OH-H₂O structures. For the hemibonded structure, thought to be responsible for the CT_{val} spectral feature in the UV-visible spectrum [11,12], the oscillator strength for the local $X \rightarrow A$ valence transition is five times smaller than that of the CT_{val} transition. In contrast, the oscillator strength for the CT_{core} transition is ~ 50 times smaller than that of the LT_{core} due to the poor overlap of the lone pair of water with the compact $1s_O$ orbital of OH.

In summary, we have measured RIXS of the short-lived hydroxyl radical in pure liquid water. At the OH resonance of 526 eV, an energy-loss feature at 3.8 eV, corresponding to the localized $X \rightarrow A$ transition of OH(*aq*), was observed. The position of the OH resonance relative to bulk water XES provides information relevant to the long-standing debate on the structural versus dynamical interpretation of water XES. *Ab initio* calculations reproduce the positions, relative intensity, and broadening of the quasielastic and energy-loss peaks of OH(*aq*) and OH⁻(*aq*) and provide insight into the relative intensities of the local and CT RIXS transitions. Time-resolved RIXS on femtosecond time-scales, enabled by the availability of intense tunable

ultrafast x-ray pulses from XFELs, highlights the localized transition in this transient species, which is otherwise hidden in direct UV absorption spectra. This ability to report on intrinsic electronic structure of OH, rather than on the properties of the solvent and its structure (as revealed by the CT transitions dominating the UV spectrum), represents the key advantage of RIXS, demonstrating that it may be used to track ultrafast reactions of the chemically aggressive hydroxyl radical in aqueous and potentially more complex environments.

This work was supported by the U.S. Department of Energy, Office of Science, Basic Energy Science, Chemical Sciences, Geosciences and Biosciences Division that supported the Argonne group under Contract No. DE-AC02-06CH11357. Use of the Linac Coherent Light Source (LCLS), SLAC National Accelerator Laboratory, and resources of the Center for Nanoscale Materials (CNM), Argonne National Laboratory, are supported by the U.S. Department of Energy (DOE), Office of Science, Office of Basic Energy Sciences (BES) under Contracts No. DE-AC02-76SF00515 and No. DE-AC02-06CH11357. L. Y. acknowledges support from Laboratory Directed Research and Development (LDRD) funding from Argonne National Laboratory for conceptual design and proposal preparation. L. K., J.-E. R. acknowledge support from the Swedish Science Council (Grant No. 2018-04088). L. K. was also supported by the European X-ray Free Electron Laser. Z.-H. L., T. D., and M. S. B. M. Y. acknowledge support from the Singapore Ministry of Education (MOE2014-T2-2-052, RG105/17, and RG109/18). M. S. was supported by the CNRS GotoXFEL program. C. A. and R. S. were supported by the Cluster of Excellence “Advanced Imaging of Matter” of the Deutsche Forschungsgemeinschaft (DFG)—EXC 2056—Project ID No. 390715994. R. S. acknowledges support by the Chemical Sciences, Geosciences, and Biosciences Division, Office of Basic Energy Sciences, Office of Science, U.S. Department of Energy, Grant No. DE-SC0019451. M. L. V. and S. C. acknowledge support from DTU Chemistry (start-up PhD grant). S. C. acknowledges support from the Independent Research Fund Denmark DFF-RP2 Grant No. 7014-00258B. At USC, this work was supported by the U.S. National Science Foundation (Grant No. CHE-1856342 to A. I. K.). A. I. K. is also a grateful recipient of the Simons Fellowship in Theoretical Physics and Mildred Dresselhaus Award from the Hamburg Centre for Ultrafast Imaging, which supported her sabbatical stay in Germany.

*krylov@usc.edu

†young@anl.gov

[1] I. S. A. Isaksen and S. B. Dalsøren, *Science* **331**, 38 (2011).[2] D. M. Rank, C. H. Townes, and W. J. Welch, *Science* **174**, 1083 (1971).

- [3] B. J. Robinson and R. X. McGee, *Annu. Rev. Astron. Astrophys.* **5**, 183 (1967).
- [4] K. P. Huber and G. Herzberg, *Molecular Spectra and Molecular Structure—IV. Constants of Diatomic Molecules* (Van Nostrand Reinhold, New York, 1979).
- [5] S. Stranges, R. Richter, and M. Alagia, *J. Chem. Phys.* **116**, 3676 (2002).
- [6] Y. Nosaka and A. Y. Nosaka, *Chem. Rev.* **117**, 11302 (2017).
- [7] E. Alizadeh and L. Sanche, *Chem. Rev.* **112**, 5578 (2012).
- [8] B. C. Garrett *et al.*, *Chem. Rev.* **105**, 355 (2005).
- [9] G. Czapski and B. H. Bielski, *Radiat. Phys. Chem.* **41**, 503 (1993).
- [10] S. Hamad, S. Lago, and J. A. Mejías, *J. Phys. Chem. A* **106**, 9104 (2002).
- [11] D. M. Chipman, *J. Phys. Chem. A* **112**, 13372 (2008).
- [12] D. M. Chipman, *J. Phys. Chem. A* **115**, 1161 (2011).
- [13] E. Codormiu-Hernandez, A. D. Boese, and P. G. Kusalik, *Can. J. Chem.* **91**, 544 (2013).
- [14] J.-H. Guo, Y. Luo, A. Augustsson, J.-E. Rubensson, C. Sâthe, H. Ågren, H. Siegbahn, and J. Nordgren, *Phys. Rev. Lett.* **89**, 137402 (2002).
- [15] O. Fuchs, M. Zharnikov, L. Weinhardt, M. Blum, M. Weigand, Y. Zubavichus, M. Bär, F. Maier, J. D. Denlinger, C. Heske, M. Grunze, and E. Umbach, *Phys. Rev. Lett.* **100**, 027801 (2008).
- [16] F. Hennies, A. Pietzsch, M. Berglund, A. Föhlisch, T. Schmitt, V. Strocov, H. O. Karlsson, J. Andersson, and J.-E. Rubensson, *Phys. Rev. Lett.* **104**, 193002 (2010).
- [17] Y.-P. Sun, F. Hennies, A. Pietzsch, B. Kennedy, T. Schmitt, V. N. Strocov, J. Andersson, M. Berglund, J.-E. Rubensson, K. Aidas, F. Gel'mukhanov, M. Odelius, and A. Föhlisch, *Phys. Rev. B* **84**, 132202 (2011).
- [18] Y. Harada, T. Tokushima, Y. Horikawa, O. Takahashi, H. Niwa, M. Kobayashi, M. Oshima, Y. Senba, H. Ohashi, K. T. Wikfeldt, A. Nilsson, L. G. M. Pettersson, and S. Shin, *Phys. Rev. Lett.* **111**, 193001 (2013).
- [19] V. Vaz da Cruz, F. Gel'mukhanov, S. Eckert, M. Iannuzzi, E. Ertan, A. Pietzsch, R. C. Couto, J. Niskanen, M. Fondell, M. Dantz, T. Schmitt, X. Lu, D. McNally, R. M. Jay, V. Kimberg, A. Föhlisch, and M. Odelius, *Nat. Commun.* **10**, 1013 (2019).
- [20] P. Wernet *et al.*, *Nature (London)* **520**, 78 (2015).
- [21] R. M. Jay *et al.*, *J. Phys. Chem. Lett.* **9**, 3538 (2018).
- [22] M. L. Vidal, X. Feng, E. Epifanovski, A. I. Krylov, and S. Coriani, *J. Chem. Theory Comput.* **15**, 3117 (2019).
- [23] K. Nanda, M. L. Vidal, R. Faber, S. Coriani, and A. I. Krylov, *Phys. Chem. Chem. Phys.* **22**, 2629 (2020).
- [24] T. Tokushima, Y. Harada, O. Takahashi, Y. Senba, H. Ohashi, L. G. M. Pettersson, A. Nilsson, and S. Shin, *Chem. Phys. Lett.* **460**, 387 (2008).
- [25] A. Pietzsch, F. Hennies, P. S. Miedema, B. Kennedy, J. Schlappa, T. Schmitt, V. N. Strocov, and A. Föhlisch, *Phys. Rev. Lett.* **114**, 088302 (2015).
- [26] T. Fransson, Y. Harada, N. Kosugi, N. A. Besley, B. Winter, J. J. Rehr, L. G. M. Pettersson, and A. Nilsson, *Chem. Rev.* **116**, 7551 (2016).
- [27] K. Yamazoe, J. Miyawaki, H. Niwa, A. Nilsson, and Y. Harada, *J. Chem. Phys.* **150**, 204201 (2019).
- [28] J. Niskanen, M. Fondell, C. J. Sahle, S. Eckert, R. M. Jay, K. Gilmore, A. Pietzsch, M. Dantz, X. Lu, D. E. McNally, T. Schmitt, V. Vaz da Cruz, V. Kimberg, F. Gel'mukhanov, and A. Föhlisch, *Proc. Natl. Acad. Sci. U.S.A.* **116**, 4058 (2019).
- [29] Z.-H. Loh *et al.*, *Science* **367**, 179 (2020).
- [30] W. F. Schlotter *et al.*, *Rev. Sci. Instrum.* **83**, 043107 (2012).
- [31] Y.-D. Chuang *et al.*, *Rev. Sci. Instrum.* **88**, 013110 (2017).
- [32] M. Nagasaka, T. Hatsui, T. Horigome, Y. Hamamura, and N. Kosugi, *J. Electron Spectrosc. Relat. Phenom.* **177**, 130 (2010).
- [33] A. I. Krylov, *Annu. Rev. Phys. Chem.* **59**, 433 (2008).
- [34] L. S. Cederbaum, W. Domcke, and J. Schirmer, *Phys. Rev. A* **22**, 206 (1980).
- [35] S. Coriani and H. Koch, *J. Chem. Phys.* **143**, 181103 (2015).
- [36] T. Helgaker, S. Coriani, P. Jørgensen, K. Kristensen, J. Olsen, and K. Ruud, *Chem. Rev.* **112**, 543 (2012).
- [37] K. D. Nanda and A. I. Krylov, *J. Chem. Phys.* **142**, 064118 (2015).
- [38] K. Nanda and A. I. Krylov, *J. Chem. Phys.* **149**, 164109 (2018).
- [39] F. Gel'mukhanov and H. Ågren, *Phys. Rep.* **312**, 87 (1999).
- [40] R. Faber and S. Coriani, *J. Chem. Theory Comput.* **15**, 520 (2019).
- [41] A. I. Krylov and P. M. W. Gill, *WIREs: Comput. Mol. Sci.* **3**, 317 (2013).
- [42] See the Supplemental Material at <http://link.aps.org/supplemental/10.1103/PhysRevLett.124.236001> for experimental and computational and theoretical details, computed XAS and RIXS spectra of OH⁻(aq) and OH(aq), computed Franck-Condon factors and vibrational broadening in the RIXS spectrum of OH(aq), and analysis of local and charge-transfer transitions in valence and core-level spectra of OH(aq), which includes Refs. [5, 11, 12, 15, 17, 22, 23, 29, 31–34, 37, 39–41, 43–64].
- [43] M. L. Vidal, A. I. Krylov, and S. Coriani, *Phys. Chem. Chem. Phys.* **22**, 2693 (2020).
- [44] M. L. Vidal, A. I. Krylov, and S. Coriani, *Phys. Chem. Chem. Phys.* **22**, 3744 (2020).
- [45] D. Rehn, A. Dreuw, and P. Norman, *J. Chem. Theory Comput.* **13**, 5552 (2017).
- [46] R. Faber and S. Coriani, *Phys. Chem. Chem. Phys.* **22**, 2642 (2020).
- [47] C. Hättig, O. Christiansen, and P. Jørgensen, *J. Chem. Phys.* **108**, 8331 (1998).
- [48] M. Paterson, O. Christiansen, F. Pawłowski, P. Jørgensen, C. Hättig, T. Helgaker, and P. Salek, *J. Chem. Phys.* **124**, 054322 (2006).
- [49] R. Sarangi, M. L. Vidal, S. Coriani, and A. I. Krylov, *Mol. Phys.* e1769872 (2020).
- [50] G. Herzberg, *Molecular Spectra and Molecular Structure: I. Spectra of Diatomic Molecules* (van Nostrand Reinhold, New York, 1950), Vol. I.
- [51] N. Foloppe and A. D. MacKerell, *J. Comput. Chem.* **21**, 86 (2000).
- [52] H. M. Senn and W. Thiel, in *Atomistic Approaches in Modern Biology* (Springer-Verlag, Berlin Heidelberg, 2007), Vol. 268, pp. 173–290.
- [53] Y. Shao and J. Kong, *J. Phys. Chem. A* **111**, 3661 (2007).

- [54] A. V. Luzanov, A. A. Sukhorukov, and V. E. Umanskii, *Theor. Exp. Chem.* **10**, 354 (1976).
- [55] M. Head-Gordon, A. M. Grana, D. Maurice, and C. A. White, *J. Phys. Chem.* **99**, 14261 (1995).
- [56] R. L. Martin, *J. Phys. Chem. A* **118**, 4775 (2003).
- [57] A. V. Luzanov and O. A. Zhikol, in *Practical Aspects of Computational Chemistry I: An Overview of the Last Two Decades and Current Trends*, edited by J. Leszczynski and M. Shukla (Springer, Netherlands, 2012) pp. 415–449.
- [58] F. Plasser, M. Wormit, and A. Dreuw, *J. Chem. Phys.* **141**, 024106 (2014).
- [59] F. Plasser, S. A. B  ppler, M. Wormit, and A. Dreuw, *J. Chem. Phys.* **141**, 024107 (2014).
- [60] S. Mewes, F. Plasser, A. I. Krylov, and A. Dreuw, *J. Chem. Theory Comput.* **14**, 710 (2018).
- [61] A. Allouche, *J. Comput. Chem.* **32**, 174 (2011).
- [62] V. A. Mozhayskiy and A. I. Krylov, ezSpectrum, <http://iopshell.usc.edu/downloads/>.
- [63] Y. Shao *et al.*, *Mol. Phys.* **113**, 184 (2015).
- [64] K. Nanda and A. I. Krylov, *J. Phys. Chem. Lett.* **8**, 3256 (2017).